TU Delft

Delft University of Technology

Elephant skin formation on UHPC surface

Effects of climatic condition and blast furnace slag content

Yalçinkaya, Çağlar; Copuroglu, Oguzhan

DOI
10.1016/j.conbuildmat.2020.121126

Publication date
2021

Document Version
Final published version

Published in
Construction and Building Materials

Citation (APA)
Yalçinkaya, Ç., & Copuroglu, O. (2021). Elephant skin formation on UHPC surface: Effects of climatic condition and blast furnace slag content. *Construction and Building Materials*, *268*, 1-12. [121126]. https://doi.org/10.1016/j.conbuildmat.2020.121126

Important note
To cite this publication, please use the final published version (if applicable).
Please check the document version above.

Copyright
Other than for strictly personal use, it is not permitted to download, forward or distribute the text or part of it, without the consent of the author(s) and/or copyright holder(s), unless the work is under an open content license such as Creative Commons.

Takedown policy
Please contact us and provide details if you believe this document breaches copyrights.
We will remove access to the work immediately and investigate your claim.

This work is downloaded from Delft University of Technology.
For technical reasons the number of authors shown on this cover page is limited to a maximum of 10.

Green Open Access added to TU Delft Institutional Repository

'You share, we take care!' - Taverne project

https://www.openaccess.nl/en/you-share-we-take-care

Otherwise as indicated in the copyright section: the publisher is the copyright holder of this work and the author uses the Dutch legislation to make this work public.

Construction and Building Materials 268 (2021) 121126

Contents lists available at ScienceDirect

Construction and Building Materials

journal homepage: www.elsevier.com/locate/conbuildmat

Elephant skin formation on UHPC surface: Effects of climatic condition and blast furnace slag content

Çağlar Yalçınkaya [a,b,*], Oğuzhan Çopuroğlu [b]

[a] Dokuz Eylül University, Faculty of Engineering, Department of Civil Engineering, 35160 İzmir, Turkey
[b] Delft University of Technology, Faculty of Civil Engineering and Geosciences, Section Materials & Environment, 2628 CN Delft, the Netherlands

HIGHLIGHTS

- Elephant skin formation can be seen on the casting surface of UHPC under any drying conditions.
- Elephant skin hampers the evacuation of air bubbles and results in a marked change in pore profile.
- A condition that triggers vapor condensation on the casting surface eliminates the elephant skin.
- Partial replacement of Portland cement with GGBS cannot eliminate the skinning phenomenon.

ARTICLE INFO

Article history:
Received 5 May 2020
Received in revised form 25 September 2020
Accepted 27 September 2020
Available online 21 October 2020

Keywords:
Elephant skin formation
UHPC
Superplasticizer
Slag
Microstructure

ABSTRACT

Ultra-high performance concrete (UHPC), which typically contains extremely high superplasticizer amount, tends to render a special type of dense surface layer, especially under drying conditions. Even if the inner side of fresh UHPC is still in a flowable nature, the top surface of the concrete which is exposed to ambient conditions renders a dense cover called "elephant skin" in a short time after casting. In this study, the effects of climatic conditions and ground granulated blast furnace slag (GGBS) replacement on the elephant skin formation were studied. The influence of elephant skin formation on the macropore profile was assessed by micro-computed tomography scan. Observations revealed that any drying condition that does not lead to water vapor condensation on the fresh surface can trigger the formation of elephant skin within minutes after casting. Both microscopic and micro-computed tomography investigations showed that as a result of elephant skin formation, most of the air bubbles cannot escape from the fresh matrix, and locate under the skin. These air bubbles and elephant skin itself result in a multi-layered structure in UHPC body throughout the cross-section and reduce the aesthetics of the casting surface. Increasing GGBS replacement percentage significantly reduced the superplasticizer demand which is responsible for skin formation, however, did not eliminate the problem.

© 2020 Elsevier Ltd. All rights reserved.

1. Introduction

Ultra-high performance concrete (UHPC) is a promising material that can reduce dimensions of structural elements while increasing the service life of the structure thanks to its compact microstructure as a result of very-low water to binder ratio. The use of UHPC in special engineering structures has increased all around the world in recent years. UHPC has been chosen as a main structural material for a variety of different bridge construction applications in the United States, Canada, Japan, South Korea, and European Countries [1]. Implementing fresh UHPC in the connections between prefabricated bridge components can be evaluated as one of the first examples for the era of field-cast UHPC [2]. The use of UHPC, however, is still mostly preferred in prefabricated elements. Some reasons behind this scant usage of field-cast UHPC can be listed as follows: uncontrolled climatic conditions (sun, wind, hot weather, etc.), extreme shrinkage values [3], lack of knowledge about the rheological properties which are very important during transporting and casting stages [4], its curing sensitivity comprising high hydration heat [5], and lack of standardization [6]. On the other hand, UHPC has not been widely used in engineering practice due to its high cost and environmental impact [7]. Either the partial replacement of Portland cement by high-volume pozzolanic materials such as fly ash, ground granulated blast furnace slag (GGBS), rice husk ash, or the incorporation of

* Corresponding author at: Dokuz Eylül University, Faculty of Engineering, Department of Civil Engineering, 35160 İzmir, Turkey.
E-mail addresses: caglar.yalcinkaya@deu.edu.tr (Ç. Yalçınkaya), o.copuroglu@tudelft.nl (O. Çopuroğlu).

https://doi.org/10.1016/j.conbuildmat.2020.121126
0950-0618/© 2020 Elsevier Ltd. All rights reserved.

inert fillers such as limestone powder or quarry-stone powders into UHPCs have been implemented to overcome these drawbacks [8–11]. While choosing the appropriate material for reducing the cost and environmental impact, local availability can be evaluated as the key factor. From this point of view, as well as by taking into account its benefits such as bringing significant durability and mechanical performance improvements to UHPC, it can be said that GGBS has become one of the most widely used supplementary cementitious materials in the production of UHPC [12–14].

The problems regarding the production of structural elements by using UHPC not only are valid for field-cast applications but also can be seen in the prefabrication area. UHPC, which has an extremely low water to binder ratio, contains a high dosage of cementitious materials and a high amount of fine powders such as silica fume and quartz powder. Consequently, its superplasticizer demand is several times higher than that of traditional concrete. A phenomenon called "elephant skin", therefore, can be observed on the casting surface of UHPCs as a side effect of an excessive amount of superplasticizer. Wetzel et al. [15] found that capillary suction causes enrichment of polycarboxylate ether superplasticizer and early hydration products in the uppermost ~ 50 μm. This enrichment resulted in the densification of the layer accompanied by an organic film of a few μm thicknesses on the top of it. It was reported that this skin forms within seconds or minutes after casting and can be observed under a drying environment with low relative humidity (RH). Chen et al. [16] have experimentally evaluated the different strategies for the control of elephant skin formation on UHPC surfaces under wind and radiation effects. These strategies aimed at reduction of evaporation from the surface, enhancement of early-age dimensional stability, and increase in cracking resistance. Their results showed that precautions that efficiently reduce moisture escape from the UHPC surface are the most effective ones in inhibiting elephant skin formation. Yalçınkaya and Yazıcı [3] have studied the early-age shrinkage characteristics of UHPC under arid or high RH conditions. The researchers showed that arid conditions resulted in elephant skin formation, and fly ash replacement, which caused a prominent increase in superplasticizer demand, intensified the formation of elephant skin. Moreover, it was reported that setting times could not be measured correctly as a result of elephant skin's resistance to the penetration of Vicat needle at the very-early age of UHPC. This densified top layer may impair the transition of water molecules to the gas phase in this zone as compared to that of a less dense surface layer [17]. Thus, the elephant skin can change the pore profile which is under the coupled effects of water evaporation, paste delamination, bubble buoyancy, gravity, and boundary [18].

In practice, several issues arising from elephant skin formation have been reported. Mendonca et al. [19] carried out a field-scale experimental study in the laboratory to evaluate the feasibility and effectiveness of placing a UHPC connection between two bridge deck panels. The researchers reported that elephant skin appeared on the surface when the UHPC, which had a strong thixotropic nature, was allowed to rest for only a short period. Before placing a new layer of UHPC, the researchers suggested rodding on the surface of the rested UHPC until elephant skin disappears. Riding et al. [20] discussed the cast-in-situ application of UHPC in bridge deck joints and pointed out that UHPC placement must be done monolithically to avoid any cold joints that may occur from the formation of elephant skin. Moreover, researchers reported that the bond between subsequent layers could be further hindered by the fact that the fibers will not bridge the interface between the layers as a side effect of the skin formation. The skin significantly reduces the finishability of the UHPC surface while causing ripples and surface cracking [21]. Increasing the fines content such as silica fume in the formulation of UHPC and exposure to direct sunlight and wind during the casting stage expedites the drying process thereby intensifying elephant skin formation [22].

Previous studies reported that UHPC can take shape as a multilayered material under exposure conditions leading to elephant skin formation. This undesirable formation at the very-early age of UHPC (seconds to minutes after casting) can cause several issues such as low aesthetic appearance, reduction of deaeration, difficulties in surface finishing, and the need for grinding after hardening. These adverse impacts cause important difficulties particularly in the production of structural members with a large surface area and so increased labor costs. Thus, the effects of climatic conditions of the production area on elephant skin formation should be clarified. On the other hand, it was reported that GGBS can reduce required cement content while reducing the need for superplasticizer [23] which is the main reason behind the skinning problem [15]. In this study, the effects of elephant skin formation on the pore profile of UHPC were for the first time investigated under low and high RH conditions at two different early-age temperatures. Moreover, the use of GGBS as a partial replacement of cement that reduces superplasticizer demand of the mixtures was studied to reveal its effect on elephant skin formation.

2. Experimental

2.1. Materials and mix proportions

Portland cement (CEM I 52.5 R), GGBS, and silica fume were used as cementitious materials. Portland cement was produced by ENCI Company (Heidelberg cement group) in the Netherlands. Densified silica fume was obtained at Elkem Silicon Materials. GGBS was provided by Orcem BV, the Netherlands. The main chemical compositions of the cementitious materials were determined by X-ray fluorescence spectrometry. The chemical and physical properties and particle size distributions of cementitious materials are shown in Table 1, and Fig. 1 respectively. To be able to work on a more homogenous cross-section regarding elephant skin formation, coarse aggregate, and steel fibers were not used in the formulation of UHPC. Thus, the aggregate phase was composed of 40% 0–125 μm and 60% 125–250 μm quartz by weight. The specific gravity and Mohs hardness of quartz powder were 2.65, and 7, respectively. A high-range water-reducing superplasticizer based on second-generation polycarboxylic ether (PCE) polymer with high early strength gains was used to adjust the slump-flow value of UHPC mixtures. Thanks to its structure based on carboxylic ether polymer with long side chains and short main chains, the superplasticizer combines effective dispersion and rapid absorption onto the particles to achieve good workability. It should be noted that the used superplasticizer is applicable in self-compacting concretes and UHPC according to the manufacturer's declaration. Some properties of superplasticizer are given

Table 1
Chemical composition and selected physical properties of binders.

Chemical Composition (wt %)	Cement	Silica Fume	GGBS
CaO	68.71	0.42	42.00
SiO_2	17.41	90.38	30.73
Al_2O_3	4.62	0.54	13.30
Fe_2O_3	2.75	3.09	0.54
MgO	2.49	0.67	9.44
K_2O	0.63	1.03	0.34
SO_3	2.44	0.57	1.45
Loss on Ignition	1.37	1.45	0.57
Physical Properties			
Strength Activity Index-28d (%)	–	125	100
Fineness (m^2/kg)	530	24,250	460
Specific Gravity	3.15	2.20	2.89

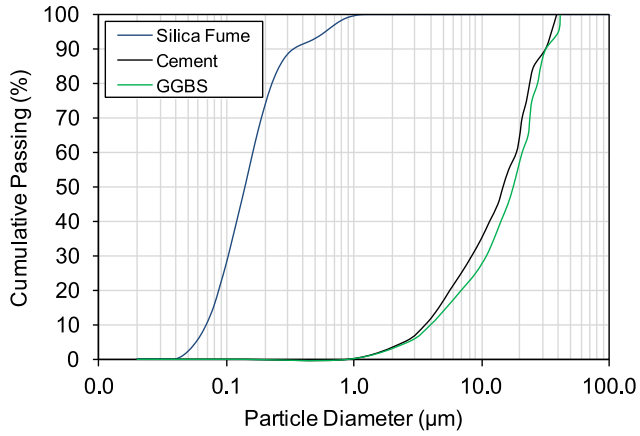


Fig. 1. Particle size distribution of cementitious materials.

Table 2
Some properties of superplasticizer.

Technical Data	Superplasticizer
Structure	Polycarboxylate ether
Color	Light brown
Physical state	Liquid
pH at 20 °C	5–8
Specific gravity	1.1
Dry content	30%

in Table 2. Indeed, different PCE based superplasticizers were tried during preliminary tests. It was observed that all of the PCE based superplasticizers led to elephant skin formation, however, the one which was more powerful on increasing slump-flow values of UHPC resulted in more prominent skinning.

A UHPC mixture endowed with the self-compacting ability was formulated as the control mixture. Silica fume was used at a dosage corresponding to 20% by weight of cement. The water to binder ratio was 0.20. In the second stage, Portland cement was replaced by 30% and 60% GGBS by weight. Thus, three UHPC mixtures were prepared. Mix proportions can be seen in Table 3. The superplasticizer dosage was adjusted to reach the target spread value (310 ± 10 mm) without segregation. Note that, the mini flow cone (60 mm high with diameters of 100 mm at the base and 70 mm at the top) was used for the slump-flow test. A Hobart mixer was used to prepare UHPC mixtures. A complicated mixing procedure was executed. First, all cementitious materials were mixed. Then, water + superplasticizer solution was added to the dry mix. After obtaining a fluid paste mixture, quartz powder was gradually included. Finally, high-speed mixing was initiated. The mixing procedure was ended in 16 min. Detailed stages of the mixing procedure are given in Fig. 2. It can be seen that to reach target workability, an extreme dosage of superplasticizer (58 kg/m^3) that can easily trigger the elephant skin formation was required for the control mixture. Note that the use of superplasticizer can be even seen at higher dosages in UHPC formulations [24,25]. Therefore, the dosage used in this study is in line with practice. GGBS replacement caused a significant reduction in superplasticizer demand. All three mixtures have shown a compressive strength of 162 ± 2 MPa at 28-day in presence of 2% steel micro fiber reinforcement.

Table 3
Mix proportions.

Materials (kg/m^3)	UHPC-C	UHPC-S30	UHPC-S60
Water	211	213	215
CEM I 52.5R	881	623	360
GGBS	–	267	540
Silica fume	176	178	180
Quartz (0–125 μm)	372	372	372
Quartz (125–250 μm)	559	559	559
Superplasticizer	58	44	30
Design Parameters			
GGBS replacement (wt.%)	0	30	60
Water to binder ratio[1]	0.20	0.20	0.20
Paste volume (%)	65	65	65
Slump-flow diameter (mm)	310 ± 10	310 ± 10	310 ± 10

[1] water/(cement + silica fume + GGBS)

2.2. Test methods and microstructural investigations

In the scope of the study, four climatic conditions were studied at early-age (≤24 h): 20 °C-95% RH, 20 °C-40% RH, 35 °C-95% RH, and 35 °C-40% RH. It was aimed to investigate elephant skin formation under moderate and hot weather conditions with low or high RH. A climate cabinet was used for this purpose. Before casting, all the raw materials and laboratory apparatus were kept under the lab condition of 20 °C at least for a week. At the end of the mixing procedure, the self-compacting mixture was poured into the molds without any vibration and put immediately into the climate cabinet which was already set to target climate condition. Although this process was completed in 1 min after the end of casting, the fresh surface was gently stirred to remove exposure history just before closing the door of the climate cabinet.

To conduct the microscopic investigation, and to make visual observations, three 40 × 40 × 160 mm^3 prismatic specimens were produced. For scanning electron microscope (SEM) investigations, polished sections were prepared after one week of curing (20 °C-99% RH). To observe cross-section, prismatic specimens were cut into pieces of 40 × 40 × 10 mm^3 perpendicular to the exposed surface by using a specially designed blade saw for cementitious materials. For backscattered electron (BSE) microscopy, nearly 20 × 20 × 10 mm^3 specimens were ground and polished. Between each step of grinding, an ultrasonic bath in the water was applied for 5 s. The microstructure of specimens was monitored by using a Philips XL30 SEM at 15 kV accelerating voltage.

Micro-computed tomography scan (CT-scan) was carried out to be able to see the profile of macropores by depth by using a Phoenix Nanotom CT-Scanner. CT-Scanner consists of an X-ray source, a rotating turntable to hold the specimen, and a detector. The cone beam of X-rays is projected onto the specimen. The different components inside the concrete specimen absorb X-rays differently, depending on their state and chemical composition. When the signals arrive at the detector located behind the concrete specimen, it brings information about X-ray absorption in the specimen. CT images are 3D maps of X-ray absorption in a specimen. Multiple X-ray images of a specimen are taken at different angles. 3D image of the internal structure of a specimen is produced by using a reconstruction algorithm. The resolution of the machine was adjusted to a voxel-size of 17.5 μm. Specimens were prepared as a cylinder with a diameter of 33.5 mm and a height of 40 mm to perform the CT-scan. Note that since the elephant skin formation is directly related to the factors which affect the drying kinetics of a specimen, the CT-scan specimens had the same volume to drying surface area ratio (40 mm) with the prismatic specimens. Specimens were exposed to the aforementioned early-age climatic conditions for 24 h and analyzed up to 20 mm depth from the casting surface. After reconstruction and obtaining 3D images of the specimens, 2D images of the slices in parallel to the casting surface were created. Then, these slices were analyzed to calculate geometrical properties (quantity, average ferret diameter, and total

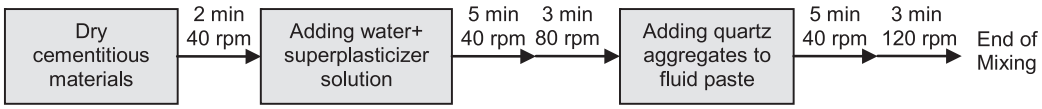


Fig. 2. Mixing procedure.

area) of macropores larger than 87.5 μm (5 times of voxel-size) by using Image-J software.

3. Results and discussion

3.1. Visual examination

UHPC mixtures achieved the target slump-flow value without segregation. Note that the slump-flow test was performed on the laboratory condition of 20 °C-40% RH. In three to five minutes after the slump-flow test, the fresh mortar was covered by a dense layer called "elephant skin" (Fig. 3). This premature densification hindered the escapes routes of air bubbles from the surface and kept them entrapped. When the surface was scraped by finger, the fresh mortar could be seen under the skin. Moreover, as a result of pulling out the skin, wrinkles that are indicators of viscoelastic behavior can be observed. This behavior makes it almost impossible to properly finish and trowel the surface.

Typical appearances of casting surfaces (~40 × 160 mm^2) subjected to four different climatic conditions at early-age (24 h) are given in Fig. 4, Fig. 5, and Fig. 6, for UHPC-C, UHPC-S30, and UHPC-S60 mixtures, in sequence. Drying environments with a 40% RH resulted in the prominent formation of elephant skin, which holds huge numbers of air bubbles beneath it. GGBS replacement reduced the diameter of observable air bubbles on the surface but apparently increased their numbers. Surface appearances of the specimens subjected to 20 °C-40% RH, and 35 °C-40% RH were similar. The climatic condition of 20 °C-95% RH also led to elephant skin formation; however, this layer can be distinguished vaguely. Moreover, these surfaces have fewer air bubbles entrapped by the skin. GGBS replacement increased the visible pores under the skin at this climatic condition. When it comes to 35 °C-95% RH, elephant skin formation could not be observed. Chen et al. [16] reported that the most effective way to inhibit elephant skin formation is the one that can stop moisture escape from the surface, e.g., to cover the surface with a plastic sheet immediately. Similarly, a dependence of this skinning on lower humidity throughout the early curing was found by Wetzel et al. [15]. In this study, 20 °C-95% RH did not lead to vapor condensation, whereas 35 °C-95% RH resulted in condensation on the surfaces. It can be said that vapor condensation inhibited evaporation from fresh UHPC and so hindered the skin formation.



Fig. 3. Elephant skin formation just after slump-flow.

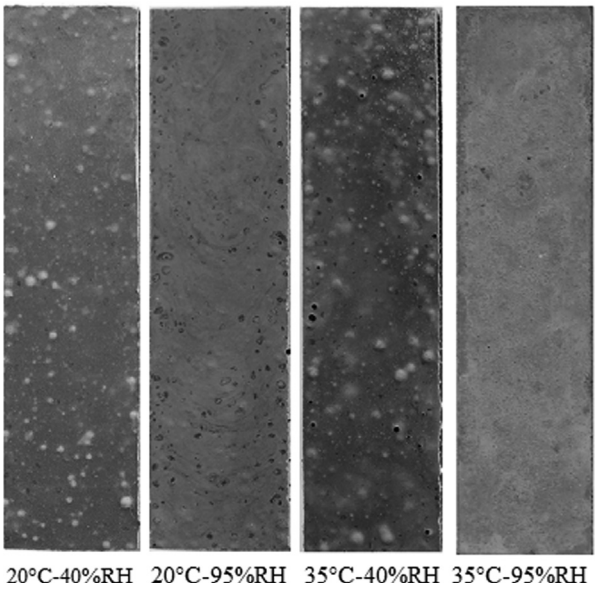


Fig. 4. Surface appearances of UHPC-C mixture depending on climatic condition.

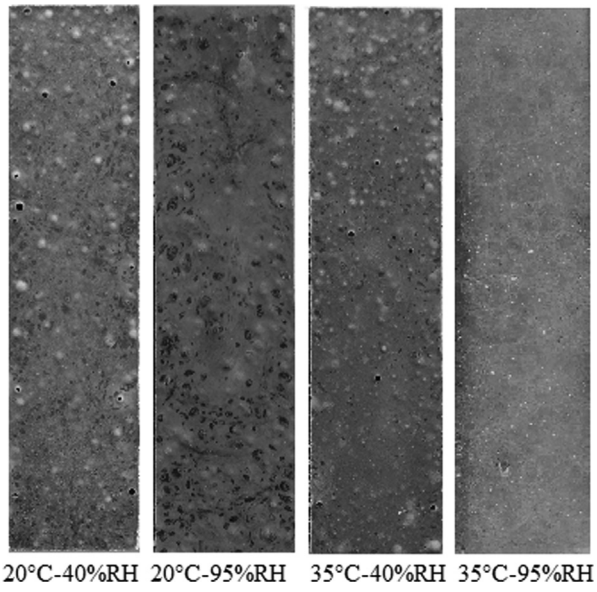


Fig. 5. Surface appearances of UHPC-S30 mixture depending on climatic condition.

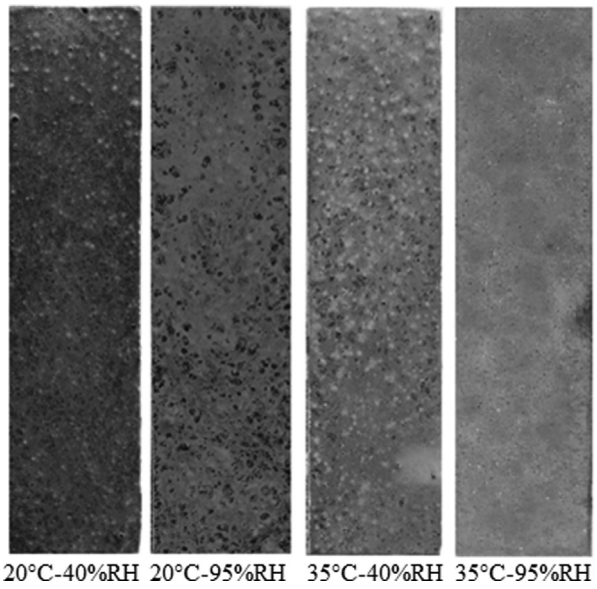


Fig. 6. Surface appearances of UHPC-S60 mixture depending on climatic condition.

3.2. CT-Scan analyses

Examples of 3D visualization of porosity and 2D slices containing pores that have Feret diameter larger than 87.5 μm can be seen in Fig. 7 obtained by using a micro CT-scan at 17.5 μm. The average circularity factor of the pores was found higher than 0.8 for each climatic condition. The lowest circularity factor was found 0.74 among the slices. In other words, porosity has comprised of mostly spherical pores as can be easily noticed in Fig. 7. This can be attributed to paste-rich UHPC's high superplasticizer dosage which tends to entrain air bubbles [26,27].

Quantity, average diameter, and area ratio of pores larger than 87.5 μm which were calculated on 2D slices by Image-J software are presented in Fig. 8, Fig. 9, Fig. 10, Fig. 11, Fig. 12, and Fig. 13 depending on climatic conditions at early-age. It can be seen from Fig. 8 and Fig. 9 that the drying environment with a low RH caused a prominent increment in the pore area on the locations close to the surface of UHPC-C mixture. This increment of pore area just beneath the surface came into existence mostly due to the synergetic effect of an increase in both pore diameter and quantity. According to Wetzel et al. [15], enrichment of PCE driven by capillary suction creates both an organic film that is only has a few μm thicknesses on the top surface, and a thicker layer with early-hydration products beneath the film. Thus, the air void profile can be attributed to elephant skin formation observed within minutes after casting. The skin holds the mobile air bubbles which move towards the surface. Besides, an increment of pore diameter under the skin can be attributed to the coalescence of some air bubbles beneath the elephant skin. In this study, 35 °C-95% RH caused condensation of humid air on the surface and completely hindered the formation of elephant skin whereas the climatic condition of 20 °C-95% led to a weak elephant skin formation despite its high humidity. The climatic condition of 20 °C-95% might give rise to a sudden drying on the surface before achieving humidity equilibrium. Since bleeding is almost impossible in UHPC that have extremely low water to binder ratio, the moisture on the UHPC surface tends to evaporate rapidly once exposed to air [28].

As a result of the replacement of Portland cement by GGBS, a similar trend of air void area was observed through cross-section (Fig. 10, Fig. 11, Fig. 12, and Fig. 13). Independent from the temperature, reducing ambient RH caused an increase in the air-void area in the shallow sections. However, the depth where the air void area was started to differentiate depending on the reduction in ambient RH shifted from around 6 mm to around 9 mm in the case of both 30% and 60% GGBS replacement.

Similar to UHPC-C mixture, slag-bearing mixtures also showed a steep rise in air void area from the depth of 2 mm to the surface at 20 °C (Fig. 8, Fig. 10, and Fig. 12). This is mainly because of an increase in the average diameter of pores accompanied by an increase in the number of pores at the relevant section. In the case of each 30% GGBS replacement, the air void area was increased by about 4% around the surface under the condition of 20 °C-95% RH. When we look into Figs. 4, 5, and 6, an increment of the number of the visible pores by GGBS replacement can be easily differentiated on the surface. Similarly, it can be seen from CT-scan results that the number of pores around the surface was markedly increased as a result of GGBS replacement. It seems GGBS replacement expedited the development of elephant skin and consequently increased the number of trapped air bubbles by limiting the time for evacuation even under the high RH condition (20 °C-95%). This can be attributed to a reduction in bleed water due to less superplasticizer demand, increased fineness of the blended system, and increased rate of evaporation in connection with less chemically bound water at a very early age [3] as a consequence of GGBS replacement. Thus, even under a high RH condition that does not induce condensation, until the UHPC surface and surrounding air reaches an RH equilibrium, a sudden surface drying due to GGBS replacement may trigger the formation of elephant skin.



Fig. 7. 3D visualization of porosity (a), 2D slice image after thresholding (b).

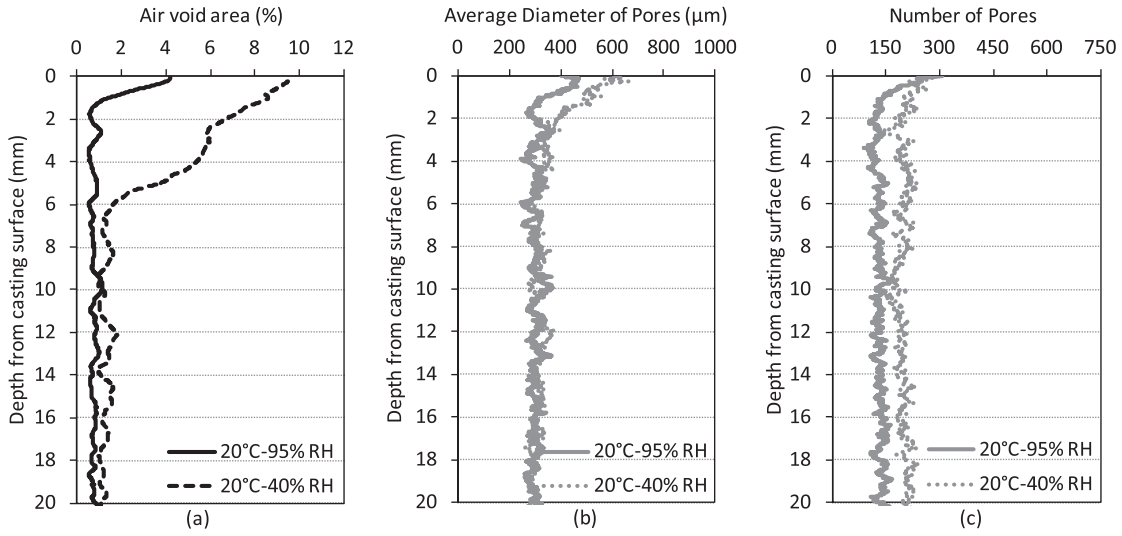


Fig. 8. Air void area (a), average pore diameter (b), and the number of the pores (c) by depth from the casting surface of UHPC-C at 20 °C.

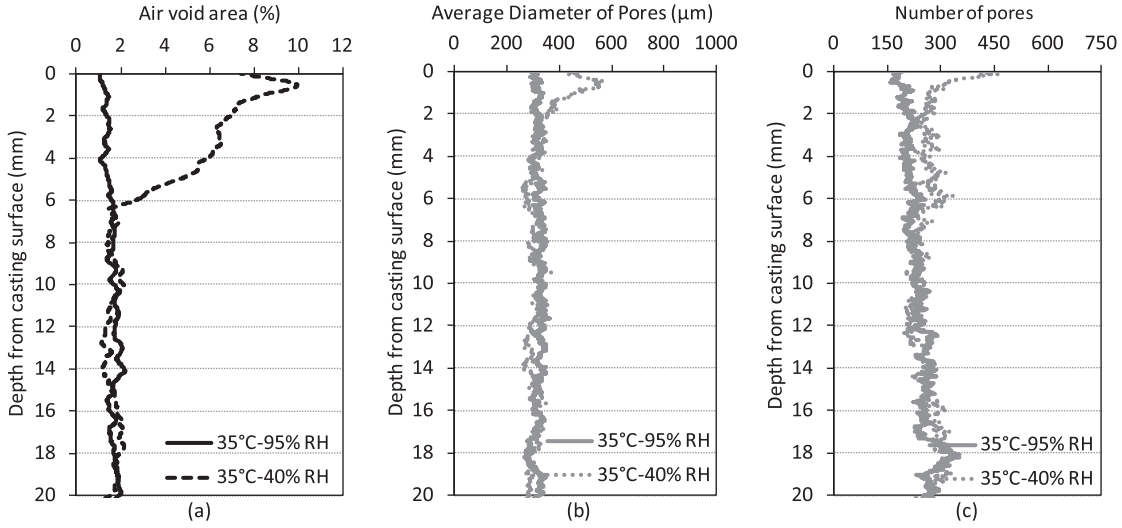


Fig. 9. Air void area (a), average pore diameter (b), and the number of the pores (c) by depth from the casting surface of UHPC-C at 35 °C.

When it comes to 35 °C, the air void area throughout the cross-section remained almost constant under 95% RH for all mixtures (Fig. 9, Fig. 11, and Fig. 13). It means there is no any skin formation that changes the pore profile by depth. This finding is supported by the surface appearances which do not reflect any elephant skin (Figs. 4, 5, and 6 at 35 °C-95% RH). In the case of 35 °C-40% RH condition, GGBS replacement weakened the uptrend of air void area slightly mainly by reducing the average diameter of pores. Because of GGBS replacements, the air void area around the surface was reduced approximately from 8% to 6%.

Elephant skin formation can be seen under any drying environment, even including a relatively high RH (95%), where any condensation that inhibits evaporation from the casting surface does not occur. Regardless of GGBS percentage, this phenomenon resulted in a significant change in pore profile consisting of mostly spherical ones through the cross-section. The air void area started to increase from the approximate depths of 6–9 mm and 2 mm to the casting surface for low (40%) and high (95%) RH conditions, respectively. Where the temperature of surrounding air having a high RH (35 °C-95% RH) was more than that of fresh UHPC (~20 °C), vapor condensation occurred on the casting surface. This hindered elephant skin formation by inhibiting evaporation from the surface. In this case, UHPCs all exhibited almost a constant air void area through the cross-section.

3.3. SEM observations

BSE images of UHPC-C mixture stored at different early-age climatic conditions are given in Fig. 14. Note that after early-age exposure conditions, the specimens were subjected to moisture curing for 7 days. It can be easily distinguished that there is no segregation or sedimentation of quartz aggregates despite the high flowability of the self-compacting mixture. Some agglomerated silica fume particles were detected on the cementitious matrix. In parallel to CT-scan results, lots of spherical air voids were found beneath the surface layer as a result of elephant skin formation under drying conditions. Some of these spherical air voids could reach a few mm diameters under a low RH condition and could locate just 80–100 μm below the surface (Fig. 14-b,d).

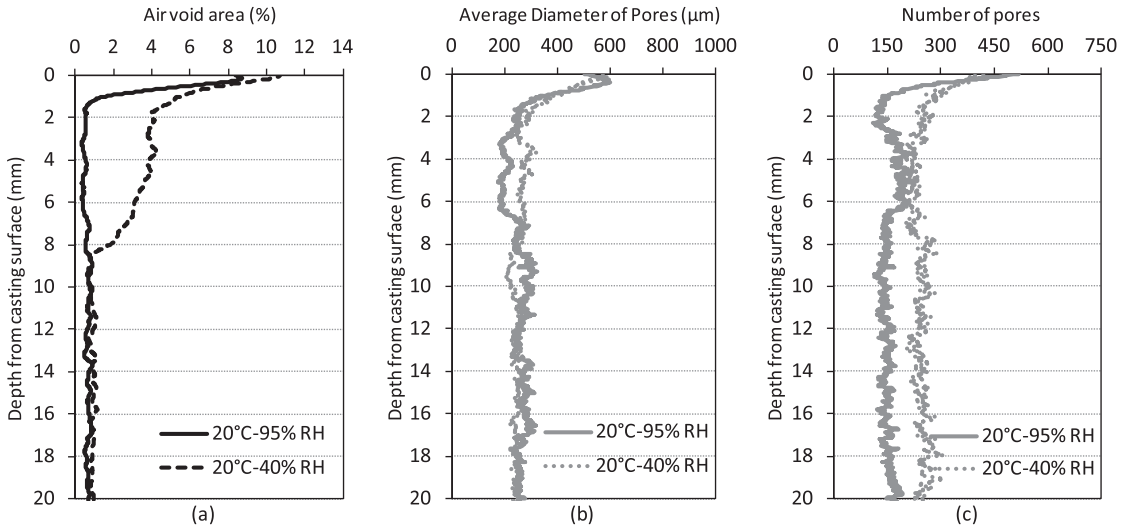


Fig. 10. Air void area (a), average pore diameter (b), and the number of the pores (c) by depth from the casting surface of UHPC-S30 at 20 °C.

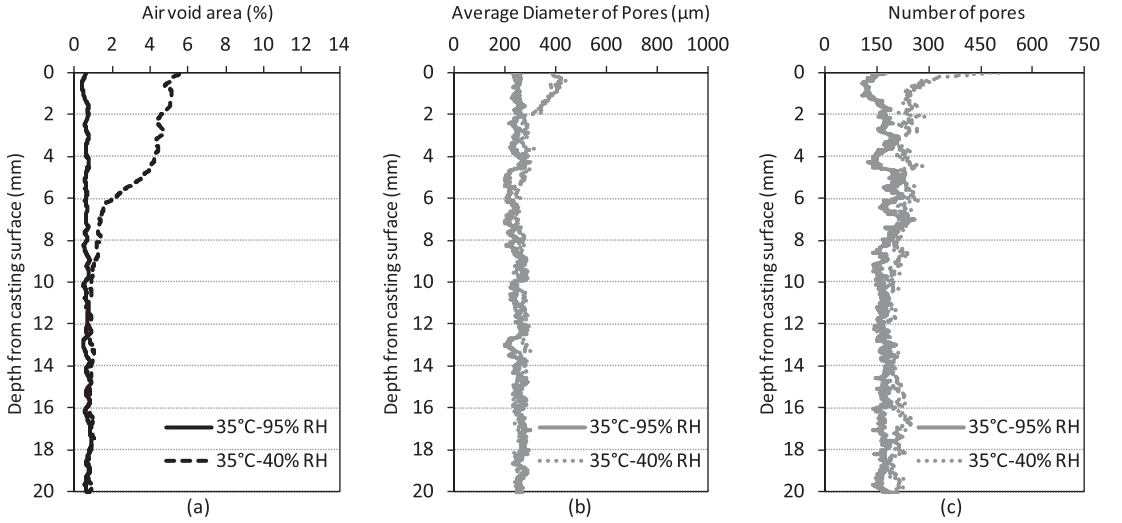


Fig. 11. Air void area (a), average pore diameter (b), and the number of the pores (c) by depth from the casting surface of UHPC-S30 at 35 °C.

BSE images of 30% and 60% GGBS replaced UHPC matrices were given in Fig. 15, and Fig. 16, respectively. It can be easily seen that there are still huge numbers of unreacted slag particles after 7 days of moisture curing as expected. Slag particles can be distinguished as sharp-edged brighter particles in the matrices. The early densification of the casting surface did not allow air bubbles to escape from the matrix containing GGBS. The condition of 35 °C-95% RH caused some open porosity on the surface of slag-bearing UHPCs. An irregular cavity and a spherical pore can be seen on the surface in Fig. 15-c and Fig. 16-c, respectively. In the case of 35 °C-95% RH, only a limited number of air bubbles were observed under the casting surface in parallel to CT-scan findings. In the case of 35 °C-40% RH, spherical macropores right under the casting surface were observed. When a prematurely hardened cementitious wall between the pores and surrounding is too thin, it can be broken and these enclosed pores may turn into open ones as observed in Fig. 16-d.

A semi-transparent and shiny layer at the top surface can be distinguished by the naked eye in Figs. 3–6 at both the fresh and hardened state of UHPCs. This is an organic film that mostly consists of superplasticizer molecules as reported by Wetzel at all [15]. During SEM observations, it was realized that the organic film layer could be easily deteriorated during sawing and polishing operations due to mechanical abrasion and chemicals that are needed for polishing. Accordingly, a new strategy was implemented to be able to observe it. First, a three-point bending test was performed on the prismatic specimen to obtain a fractured cross-section perpendicular to the casting surface. After that, a sample containing a region of the casting surface was extracted from the cross-section. Due to the organic nature of PCE based superplasticizer, it was not possible to detect the film layer that was arisen from the enrichment of superplasticizer under BSE mode. When it comes to the SE image, the film layer, which was not observable on the BSE image, could be clearly observed on the uppermost (Fig. 17). When the specimens were observed from their upper side, some pop-out-like cavities were found on the smooth surface (Fig. 18-a). These pop-outs can be attributed to the top layer's extreme deformation arising from drying shrinkage of the surface that was directly exposed to the drying environment.

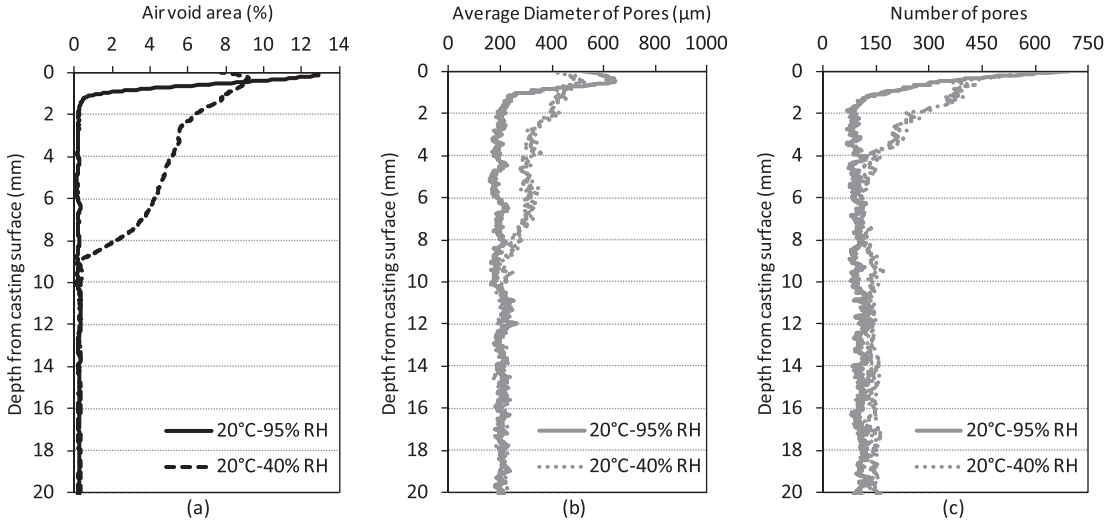


Fig. 12. Air void area (a), average pore diameter (b), and the number of the pores (c) by depth from the casting surface of UHPC-S60 at 20 °C.

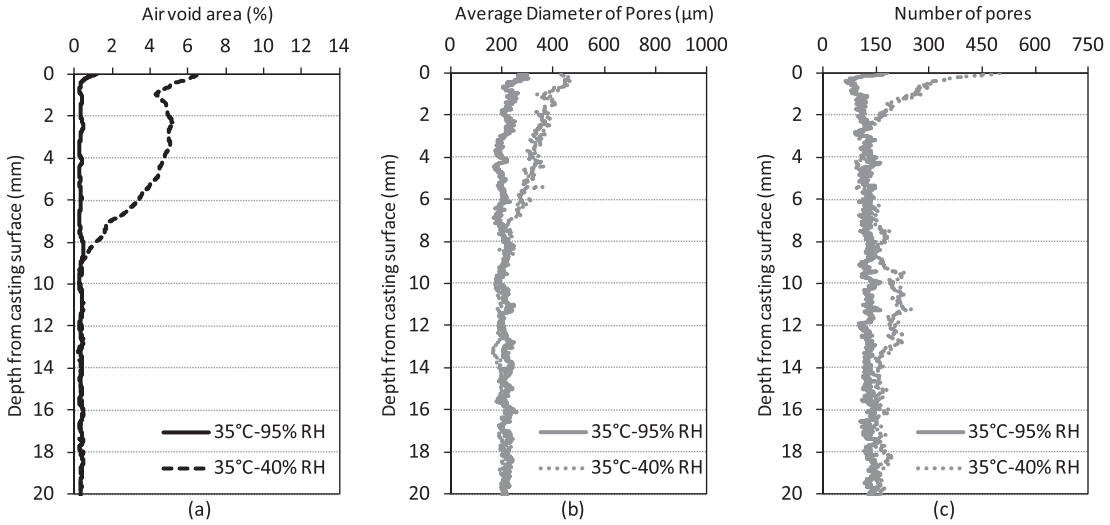


Fig. 13. Air void area (a), average pore diameter (b), and the number of the pores (c) by depth from the casting surface of UHPC-S60 at 35 °C.

It can be seen that the uppermost of the casting surface was covered by a thin and smooth layer (Fig. 18-b), and there were several unreacted particles as well as inert materials like quartz grains under it. The uppermost layer apparently contains hydration products that cause early densification. Similarly, Lee et al. [29] observed a smooth surface which can cause some cold-joint issues during the casting process of UHPC. They concluded that the film formed on the casting surface consists of SiO_2 crystalline structures and that this is the cause of the degradation of the bonding performance in terms of cold-joint formation. It is believed that the smooth surface reported was mostly due to elephant skin formation accompanied by an organic film at the top.

3.4. Illustration of the mechanism

Based on observations and the previous findings [15,16], the mechanism of elephant skin formation and the multi-layered structure of UHPC can be illustrated as in Fig. 19. The drying environment, which UHPC was subjected to, leads to evaporation from the surface and generates an extreme capillary suction around the surface. As a result, the pore solution which is superplasticizer-rich is transported to the surface, and the superplasticizer enriches on the top surface as a film layer. During that time, early hydration products also enrich on the surface. Contraction forces that are driven by mostly drying make upper layers very dense. Early hydration products, contraction forces, and the film layer on the top lead to the densification of fresh UHPC surface within minutes after casting, which is called elephant skin [15]. Note that this skin can even resist the penetration of Vicat needle much earlier than the initial setting time [30]. Elephant skin acts as a barrier that obstructs evacuation of air bubbles in the flowable matrix. At the end of this undesirable quick process, the cross-section of UHPC can be observed in three layers as illustrated in Fig. 19-a. In the hardened state, the uppermost layer which has a few micrometers thickness can be distinguished as a shiny cover by the naked eye. The second layer beneath the first one contains lots of entrapped air bubbles which some of them coalesced forming larger bubbles right under the first layer. The second layer may have a depth of a few millimeters. Thanks to its low macroporosity, the third layer has a more compact appearance than the second one as expected

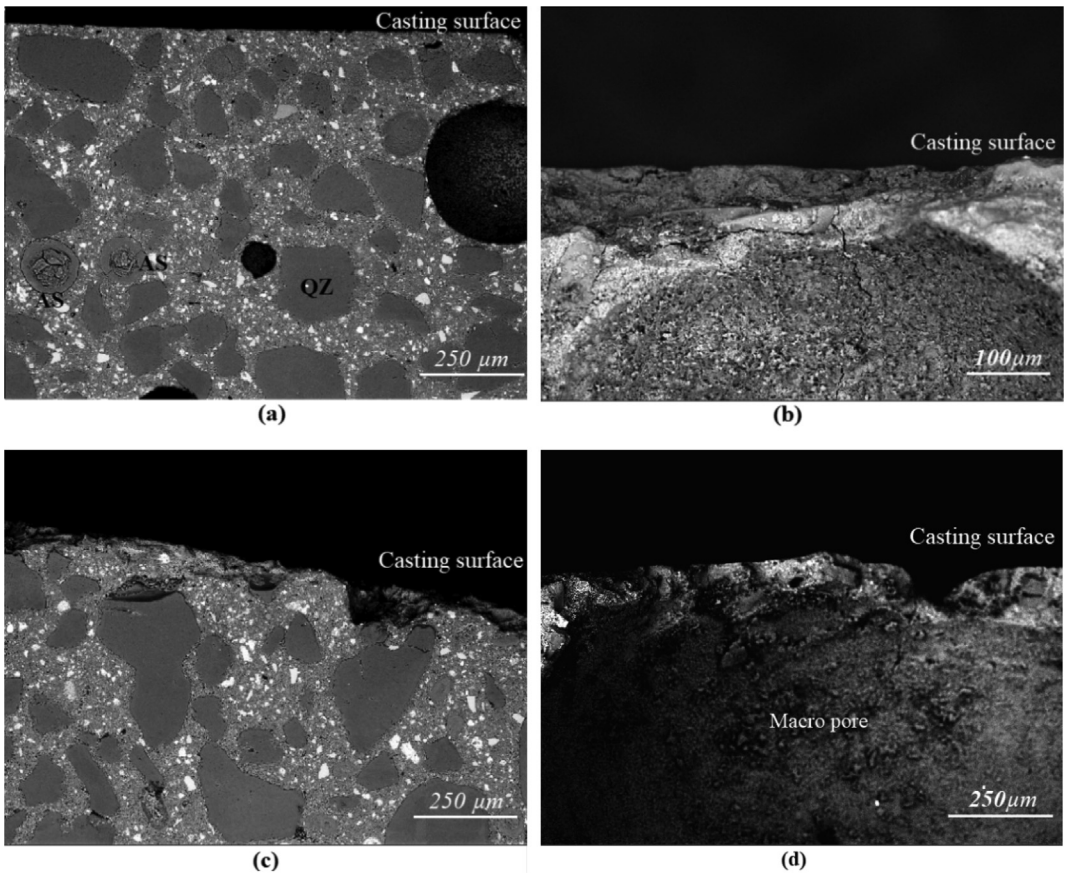


Fig. 14. BSE micrographs of UHPC-C stored at 20 °C-95% RH (a), 20 °C-40% RH (b), 35 °C-95% RH (c), and 35 °C-40% RH (d). (QZ: quartz, AS: agglomerated silica fume).

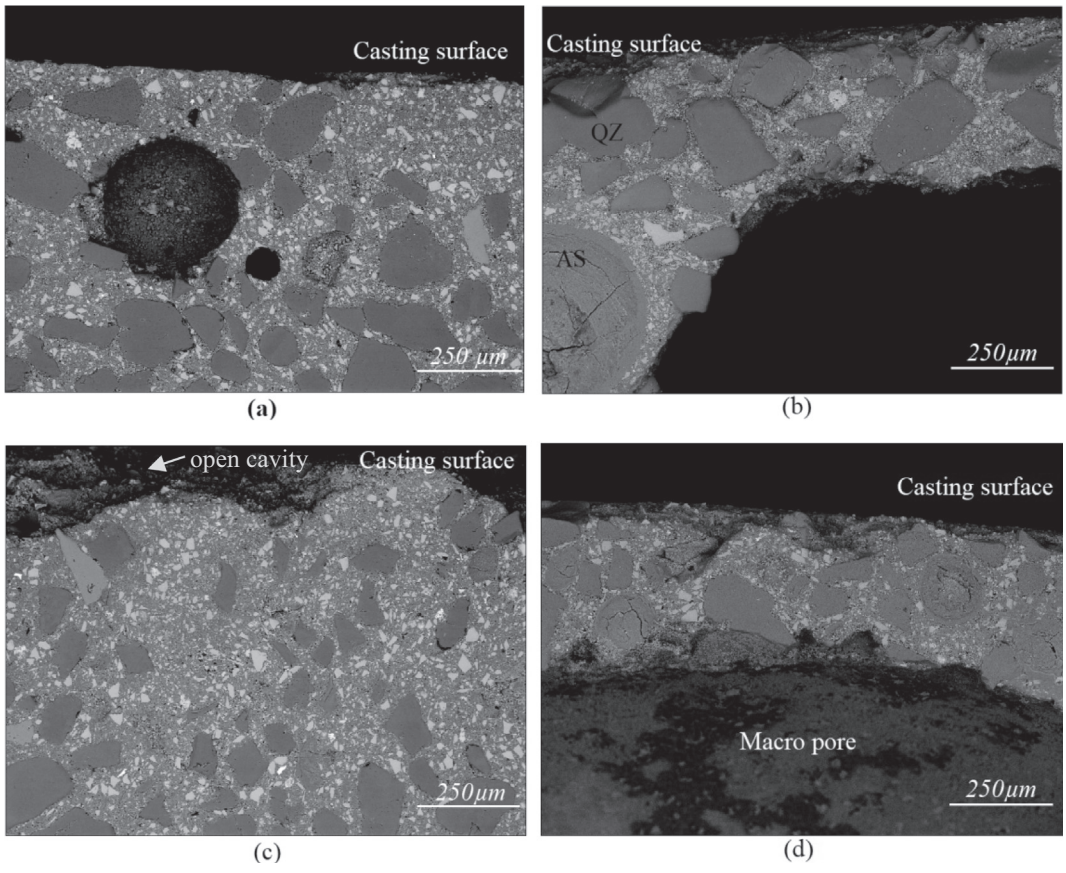


Fig. 15. BSE micrographs of UHPC-S30 stored at 20 °C-95% RH (a), 20 °C-40% RH (b), 35 °C-95% RH (c), and 35 °C-40% RH (d). (QZ: quartz, AS: agglomerated silica fume).

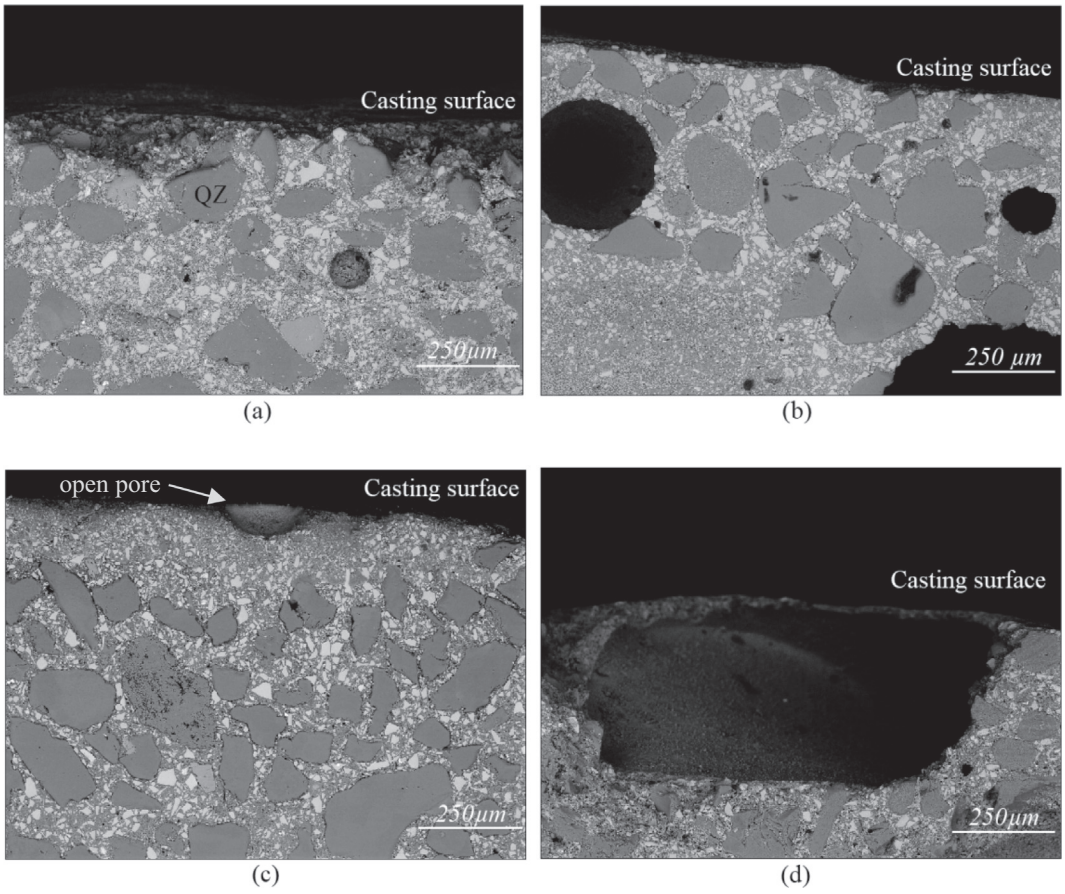


Fig. 16. BSE micrographs of UHPC-S60 stored at 20 °C-95% RH (a), 20 °C-40% RH (b), 35 °C-95% RH (c), and 35 °C-40% RH (d). (QZ: quartz).

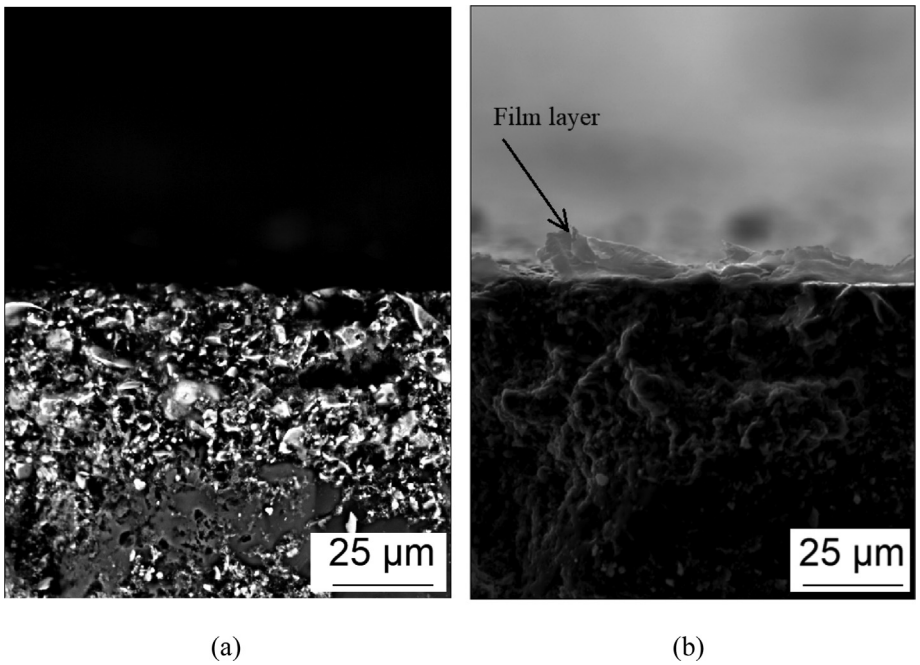


Fig. 17. Typical BSE (a) and SE (b) micrographs of the organic film layer (UHPC-C at 35 °C-40% RH).

from a UHPC. If evaporation of the mix water from the casting surface is inhibited by implementing a sealing method such as immediately covering by a plastic sheet [16,31], elephant skin formation can be prevented (Fig. 19-b). Moreover, according to our findings, vapor condensation on the casting surface impedes the formation of elephant skin completely.

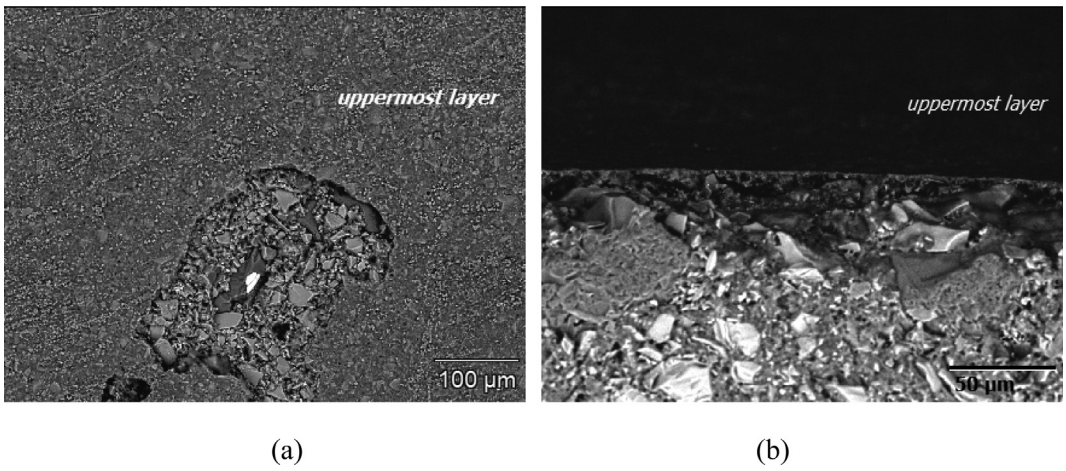


Fig. 18. BSE micrographs from above (a) and cross-section (b) (UHPC-S60 at 35 °C-40% RH).

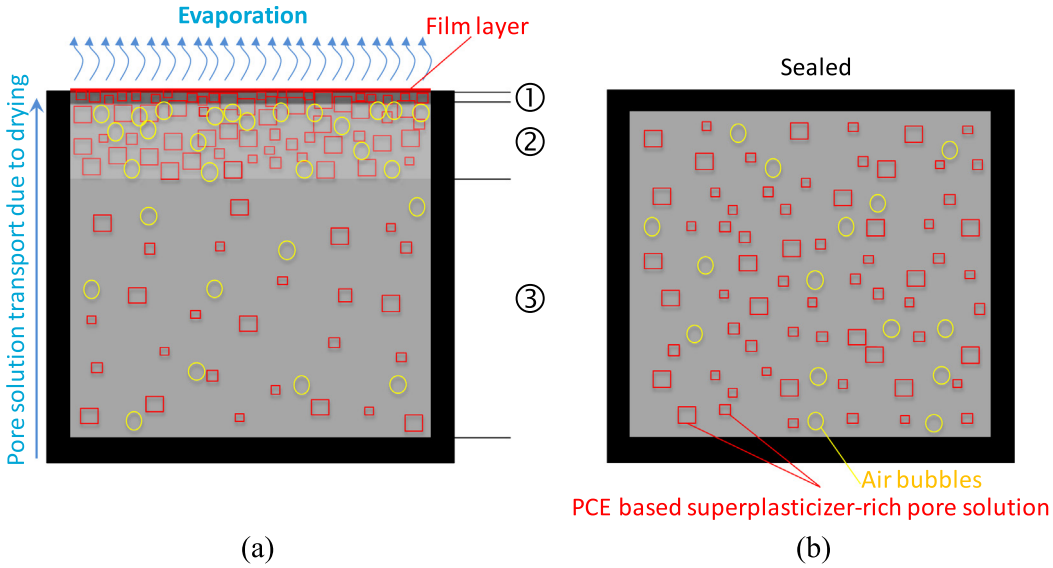


Fig. 19. Illustration of elephant skin formation and multi-layered structure of UHPC (a), prevention of elephant skin (b) (①organic film layer and dense zone due to enrichment of superplasticizer + early hydration products + contraction, ②porous zone due to hindered deaeration, ③the bulk of UHPC).

4. Conclusions

To unravel the effects of early-age climatic conditions and GGBS replacement on the skinning problem of UHPC colloquially described as "elephant skin formation", an experimental study has been conducted. The following major conclusions can be drawn;

1) Elephant skin formation can be seen on the casting surface of UHPC in just a few minutes under any drying condition. It was observed that even a humid-rich environment with an RH of 95% could not hinder the formation at 20 °C. The early age exposure condition of 35 °C-95% RH that triggered vapor condensation on the casting surface eliminated evaporation thereby inhibiting the skinning phenomenon.
2) Increasing GGBS replacement percentage reduced markedly PCE based superplasticizer demand which is responsible for the skinning, however, did not eliminate the problem. Elephant skin formation hampered the evacuation of air bubbles and resulted in a significant change in pore profile consisting of mostly spherical ones through the cross-section. Independent from temperature, reducing ambient RH caused an increase in the air-void area in the shallow sections. The air void area started to increase from the approximate depths of 6–9 mm and 2 mm to the casting surface in the case of low (40%) and high (95%) RH conditions, respectively. A huge number of air bubbles can locate just 80–100 μm below the surface, and result in roughen and non-aesthetic surface appearance. In the condition of 35 °C-95% RH that inhibits the skinning problem, UHPCs all exhibited almost a constant air void profile by depth.
3) As a result of elephant skin formation, a smooth surface at a micro-scale was observed. Under this surface cover, there were lots of unreacted cementitious materials. This premature formation may cause cold-joint problems at even very-early age by reducing the bond properties between consecutive layers.

For the precast industry, it can be a solution to cast UHPC into the molds under a controlled climatic condition that causes vapor condensation on the casting surface. Moreover, some modifications on the molds systems that reduce the evaporation area by enabling

vertically casting of reinforced concrete members such as slabs and beams can be made. On the other hand, the potential problems related to elephant skin formation in the cast-in-situ application of UHPC should be also meticulously taken into account during the standardization period.

CRediT authorship contribution statement

Çağlar Yalçınkaya: Conceptualization, Methodology, Investigation, Visualization, Funding acquisition, Writing - original draft. **Oğuzhan Çopuroğlu:** Supervision, Methodology, Resources, Investigation, Funding acquisition, Writing - review & editing.

Declaration of Competing Interest

The authors declare that they have no known competing financial interests or personal relationships that could have appeared to influence the work reported in this paper.

Acknowledgments

Çağlar Yalçınkaya would like to acknowledge the postdoctoral research fellowship supported by The Scientific and Technological Research Council of Turkey (TUBITAK). The authors would like to acknowledge Arjan Thijssen and Stefan Chaves Figueiredo for their assistance in CT-Scan experiments and Image-J analysis, respectively. The authors would like to thank Elkem Silicon Materials for material support.

References

[1] H.G. Russell, B.A. Graybeal, Ultra-high performance concrete: a state-of-the-art report for the bridge community, U.S. Department of Transportation, Federal Highway Administration, McLean, USA, 2013.
[2] B. Graybeal, Design and Construction of Field-cast UHPC Connections, Federal Highway Administration, United States, 2014.
[3] Ç. Yalçınkaya, H. Yazıcı, Effects of ambient temperature and relative humidity on early-age shrinkage of UHPC with high-volume mineral admixtures, Constr. Build. Mater. 144 (2017) 252–259, https://doi.org/10.1016/j.conbuildmat.2017.03.198.
[4] A. Sadrmomtazi, S. Tajasosi, B. Tahmouresi, Effect of materials proportion on rheology and mechanical strength and microstructure of ultra-high performance concrete (UHPC), Constr. Build. Mater. 187 (2018) 1103–1112, https://doi.org/10.1016/j.conbuildmat.2018.08.070.
[5] K. Liu, R. Yu, Z. Shui, X. Li, X. Ling, W. He, et al., Effects of Pumice-Based Porous Material on Hydration Characteristics and Persistent Shrinkage of Ultra-High Performance Concrete (UHPC), Materials (Basel). 12 (2018) 11, https://doi.org/10.3390/ma12010011.
[6] J. von Werder, S. Simon, C. Lehmann, C. Selleng, P. Fontana, B. Meng, Autoclaving of ultra-high performance concrete (UHPC), Ce/Papers. 2 (2018) 131–136, https://doi.org/10.1002/cepa.866.
[7] Y.Y. Wu, J. Zhang, C. Liu, Z. Zheng, P. Lambert, Effect of graphene oxide nanosheets on physical properties of ultra-high-performance concrete with high volume supplementary cementitious materials, Materials (Basel). 13 (2020), https://doi.org/10.3390/MA13081929.
[8] R. Yang, R. Yu, Z. Shui, X. Gao, J. Han, G. Lin, D. Qian, Z. Liu, Y. He, Environmental and economical friendly ultra-high performance-concrete incorporating appropriate quarry-stone powders, J. Clean. Prod. 260 (2020), https://doi.org/10.1016/j.jclepro.2020.121112.
[9] Z. Mo, R. Wang, X. Gao, Hydration and mechanical properties of UHPC matrix containing limestone and different levels of metakaolin, Constr. Build. Mater. 256 (2020) 119454, https://doi.org/10.1016/j.conbuildmat.2020.119454.
[10] P.P. Li, H.J.H. Brouwers, W. Chen, Q. Yu, Optimization and characterization of high-volume limestone powder in sustainable ultra-high performance concrete, Constr. Build. Mater. 242 (2020) 118112, https://doi.org/10.1016/j.conbuildmat.2020.118112.
[11] J. Xue, B. Briseghella, F. Huang, C. Nuti, H. Tabatabai, B. Chen, Review of ultra-high performance concrete and its application in bridge engineering, Constr. Build. Mater. 260 (2020) 119844, https://doi.org/10.1016/j.conbuildmat.2020.119844.
[12] M.N. Isa, K. Pilakoutas, M. Guadagnini, H. Angelakopoulos, Mechanical performance of affordable and eco-efficient ultra-high performance concrete (UHPC) containing recycled tyre steel fibres, Constr. Build. Mater. 255 (2020) 119272, https://doi.org/10.1016/j.conbuildmat.2020.119272.
[13] P. Ganesh, A.R. Murthy, Tensile behaviour and durability aspects of sustainable ultra-high performance concrete incorporated with GGBS as cementitious material, Constr. Build. Mater. 197 (2019) 667–680, https://doi.org/10.1016/j.conbuildmat.2018.11.240.
[14] Y. Shi, G. Long, C. Ma, Y. Xie, J. He, Design and preparation of ultra-high performance concrete with low environmental impact, J. Clean. Prod. 214 (2019) 633–643, https://doi.org/10.1016/j.jclepro.2018.12.318.
[15] A. Wetzel, C. Glotzbach, K. Maryamh, B. Middendorf, Microstructural investigations on the skinning of ultra-high performance concrete, Cem. Concr. Compos. 57 (2015) 27–33, https://doi.org/10.1016/j.cemconcomp.2014.11.010.
[16] Y. Chen, F. Matalkah, W. Rankothge, A. Balachandra, P. Soroushian, Improvement of the surface quality and aesthetics of ultra-high-performance concrete, Proc. Inst. Civ. Eng. Constr. Mater. 172 (2019) 246–255, https://doi.org/10.1680/jcoma.17.00009.
[17] C. Schröfl, V. Mechtcherine, D. Mannes, Dewatering kinetics from fresh cement pastes enriched with superabsorbent polymer (SAP) samples at ambient and elevated temperatures visualised and quantified by neutron radiography imaging. In: Proceedings of SAP2019, Skukuza, South Africa, 2019, pp 123–131.
[18] P. Liu, Y. Chen, F. Sha, Z. Yu, G. Shao, Study on micro structure and composition distribution of concrete surface zone based on fractal theory and XCT technology, Constr. Build. Mater. 263 (2020) 120209, https://doi.org/10.1016/j.conbuildmat.2020.120209.
[19] F. Mendonca, M.A. El-Khier, G. Morcous, J. Hu, Feasibility Study of Development of Ultra-High Performance Concrete (UHPC) for Highway Bridge Applications in Nebraska, Nebraska Department of Transportation Research Reports, 2020.
[20] K.A. Riding, C.C. Ferraro, H.R. Hamilton, M.S. Voss, R.S. Alrashidi, "Requirements for Use of Field-Cast, Proprietary Ultra-High-Performance Concrete in Florida Structural Applications" (2019). Florida Department of Transportation Research Reports.
[21] J.S. Lawler, M.K. Tadros, M. Lampton, E.N. Wagner. "Development of Non-Proprietary UHPC for Florida Precast Applications" (2019). In International Interactive Symposium on Ultra-High Performance Concrete (Vol. 2, No. 1). Iowa State University Digital Press.
[22] M. Ženíšek, T. Vlach, L. Laiblová, Dosage of silica fume in high performance concrete, Key Eng. Mater. 677 (2016) 98–102, https://doi.org/10.4028/www.scientific.net/KEM.677.98.
[23] J. Lim, S. Raman, M. Safiuddin, M. Zain, R. Hamid, Autogenous Shrinkage, Microstructure, and Strength of Ultra-High Performance Concrete Incorporating Carbon Nanofibers, Materials (Basel). 12 (2019) 320, https://doi.org/10.3390/ma12020320.
[24] M. Skazlić, S. Marijana, B. Dubravka, Influence of test specimen geometry on compressive strength of ultra high performance concrete, Kassel, Second International Symposium on Ultra High Performance Concrete, 2008, pp. 296–301.
[25] B.A. Graybeal, Field-Cast UHPC Connections for Modular Bridge Deck Elements, Federal Highway Administration (FHWA), publication no FHWA-HRT-11-022 (2010).
[26] J. Szwabowski, B. Łaźniewska-Piekarczyk, The increase of air content in SCC mixes under the influence of carboxylate superplasticizer, Cem, Wapno, Bet, 2011.
[27] X. Wang, R. Yu, Q. Song, Z. Shui, Z. Liu, S. Wu, et al., Optimized design of ultra-high performance concrete (UHPC) with a high wet packing density, Cem. Concr. Res. 126 (2019), https://doi.org/10.1016/j.cemconres.2019.105921.
[28] E. Fehling, M. Schmidt, J. Walraven, T. Leutbecher, S. Fröhlich, eds., Ultra-High Performance Concrete UHPC, Wiley, 2014. doi:10.1002/9783433604076.
[29] H.S. Lee, H.O. Jang, K.H. Cho, Evaluation of bonding shear performance of ultra-high-performance concrete with increase in delay in formation of cold joints, Materials (Basel). 9 (2016), https://doi.org/10.3390/ma9050362.
[30] Ç. Yalçınkaya, H. Yazıcı, Early-age shrinkage properties of eco-friendly reactive powder concrete with reduced cement content, Eur. J. Environ. Civ. Eng. (2019), https://doi.org/10.1080/19648189.2019.1665105.
[31] M. Rasul, S. Ahmad, S.K. Adekunle, S.U. Al-Dulaijan, M. Maslehuddin, S.I. Ali, Evaluation of the Effect of Exposure Duration and Fiber Content on the Mechanical Properties of Polypropylene Fiber-Reinforced UHPC Exposed to Sustained Elevated Temperature, J. Test. Eval. 48 (2020) 20180687, https://doi.org/10.1520/jte20180687.